Strain localization in geomaterials in nature, laboratory tests and numerical analyses

Aniruddha Sengupta

Department of Civil Engineering, Indian Institute of Technology, Kharagpur 721 302, India

Most of the failures in brittle geomaterials are associated with localization of large strains along well-defined zones. The emergence of these localized zones of high strains is a precursor to failure and hence its importance. At IIT Kharagpur, studies in progress on strain localization include biaxial tests and model tests in the laboratory, numerical analyses and field studies at landslide zones. Results of these studies reveal that strain localizations observed in nature at a landslide, captured in laboratory biaxial tests and model tests, and predicted by finite element analyses bear close resemblance to one another.

Keywords: Finite element analyses, geomaterials, landslide, plane strain tests, strain localization.

MOST of the failures in brittle geomaterials like rock, sand and overconsolidated clay are associated with localization of large strains along well-defined zones. Typically, at or near failure, strains are concentrated along these well-defined zones while the major part of a material experiences unloading. Along the zones of localization, the strains are orders of magnitude higher than the strains found in other portions of the same material. A schematic diagram of strain localization in a soil sample under compressional load is given by Vardoulakis[1] and shown in Figure 1. The intense shearing/flow reorients the random internal structures of a material and aligns them parallel to the strain localized zones. Such strain localization can be caused by geometrical effects (e.g. necking of metallic bars) or by material instabilities (e.g. microcracking, frictional slip or plastic flow). The accumulation of strains in these narrow zones is primarily responsible for the accelerated softening response exhibited by many materials at high strain level. Particular examples can be found in concrete, rocks, sand and overconsolidated clay, where progressive damage produces strain softening. The emergence of these localized zones of high strains is a precursor to failure and hence its importance. If these localized zones can be detected or predicted beforehand, precautions can be taken against failure or it can be avoided all together.

Strain localization in metals is a well studied problem and such localization of strains can be observed readily in common laboratory tests like, tensile test on cylindrical metal bars. However, in geomaterials like sand and clay, evolution of strain localization cannot be observed that easily. Some of the important researches related to the strain localization in sand are by Arthur *et al.*[2], Vardoulakis[3–5], Mühlhaus and Vardoulakis[6], Peters *et al.*[7], Drescher *et al.*[8], Finno *et al.*[9,10], Liang *et al.*[11], Saada *et al.*[12] and Alshibli *et al.*[13,14]. They have studied evolution of strain localization in triaxial and in biaxial laboratory tests on sand. Balasubramanium[15], Saada *et al.*[16], Topolnicki *et al.*[17], Finno and Rhee[18], Viggiani *et al.*[19], Hicher *et al.*[20], Sabatini and Finno[21], Lizcano *et al.*[22], Sengupta and Sengupta[23] have studied the localization in clayey materials in triaxial and biaxial laboratory tests. Rudnicki and Rice[24], Needleman[25], Prevost[26], Peric *et al.*[27], Wu[28], Lambrecht and Miehe[29] have looked at the localization problem theoretically. They have demonstrated that localization depends on factors like choice of material model, size of incremental steps in the algorithm, fineness of the finite element mesh, etc. As may be seen here, significant amount of work has been done to understand strain localization in sands and clays. But comparison between the strain localization observed in the laboratory tests and in numerical analyses is limited. Almost no reference can be cited on strain localization observed in nature and in laboratory model tests.

At the Indian Institute of Technology (IIT), Kharagpur studies on localization in geomaterials have been in progress since 2003. Studies include both the laboratory

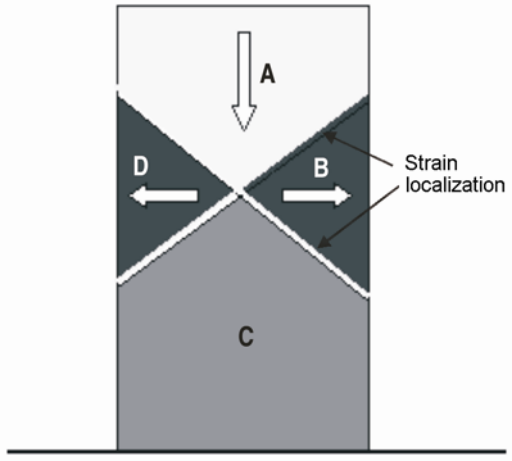

Figure 1. Schematic diagram of strain localization (after Verdoulakis[1]).

e-mail: sengupta@civil.iitkgp.ernet.in

experiments and numerical analyses on the evolution of strain localization in clayey materials as well as field studies on rocks at the landslide-prone areas in Sikkim. This article attempts to demonstrate that strain localization can be captured not only in laboratory tests and in numerical analyses, but also observed in rocks in landslide-prone zones and in simple laboratory model tests. It is also demonstrated that the strain localization and reorientation of microfabrics associated with it observed in nature, laboratory tests, numerical analyses, and in model tests are remarkably similar.

Strain localization observed in nature

The strain localization, though a natural phenomenon, is seldom observed in nature especially in soils as it is almost never preserved. However, it is not the case with rocks which experienced tremendous shearing or flow in the past. Under the sponsorship of DST, Government of India, a study of landslides in Sikkim was undertaken where soil and rock samples were collected for further classifications and analyses. The Lanta Khola slide on the North Sikkim Highway (NSH) in North Sikkim is one of the investigated landslides[30]. Figure 2 shows the location of the slide in Sikkim and a view of the slide itself. Detail geological study performed in the area reveals that the landslide is located on a fault. The fault is daylighting within the slide itself triggering the landslide. Two types of rock are found at Lanta Khola – gneiss and mica schist. Figure 3 shows the magnified view of the internal structures (thin sections) of both the rocks collected from the landslide zone and away from it. The figure reveals how, due to shear flow under intense heat and pressure during the activation of the fault in the distant past, the pre-existing structures within the rocks were wiped away and grains realigned themselves along the shear/flow (fault) direction. The orientation of the internal rock grains and the fault is found to be the same and given by N37°W strike and dipping 50°E. Interestingly, this happens to be close to the direction (N45°W strike and 45°E dip) of the Main Central Thrust (MCT), one of the major faults in the Himalayan region. Interestingly, in the laboratory tests on much softer materials like clay, similar reorientation of grains is noticeable during shearing.

Strain localization in the laboratory

Laboratory biaxial plane strain tests

A commercially available kaolinitic clay is utilized for the laboratory tests. The kaolinite being a nonswelling material in wet condition is ideal for this kind of study. Its specific gravity is 2.68. According to the Indian code (IS: 1498–1970), it is classified as CI material (intermediate plasticity clay). A uniform slurry of kaolinite is prepared in a tank and it is allowed to consolidate under a uniform pressure of 275 kPa for 15–30 days. Fully consolidated and saturated soil samples are extruded from the middle of the tank (to ensure homogeneity) with the help of a rectangular split mould for the biaxial plane strain tests.

The laboratory biaxial plane strain test cell consists of two Perspex plates of $226 \times 146 \times 25$ mm in size bolted together with a $140 \times 70 \times 25$ mm soil specimen wrapped in transparent latex membrane sandwiched between them (see Figure 4). The bottom end platen is restrained from movement and the top end platen can slide smoothly in

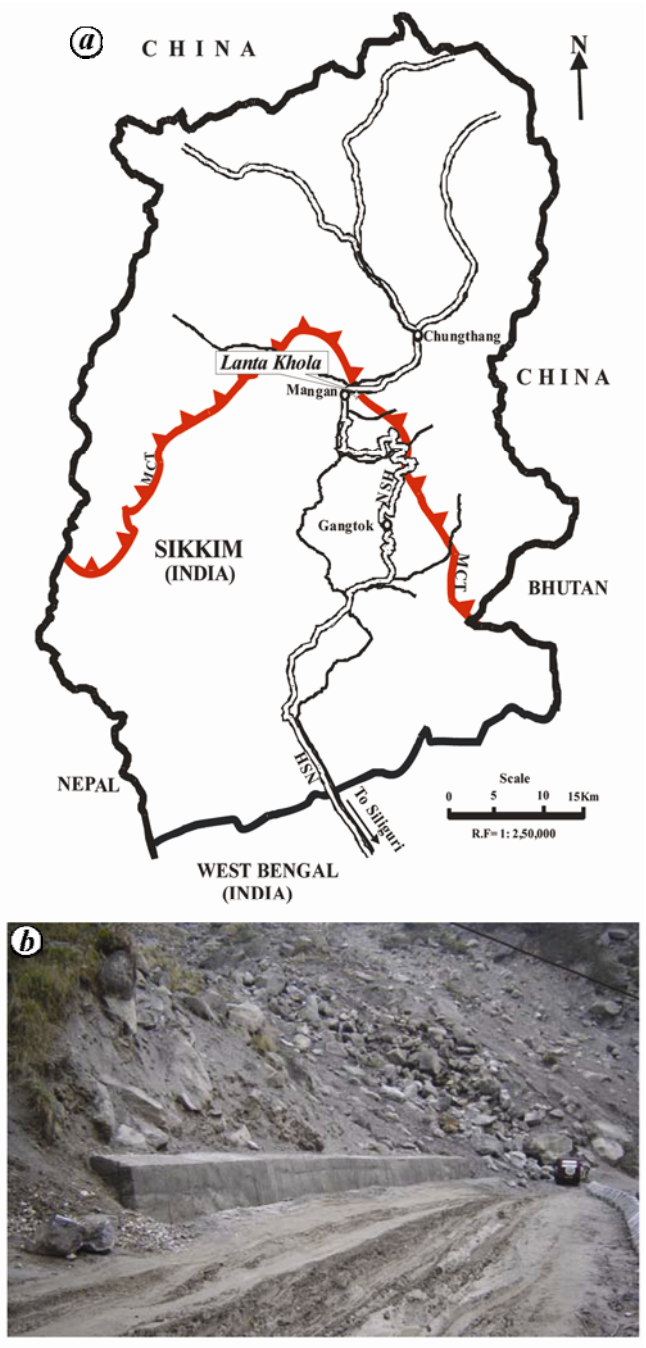

Figure 2. ***a***, Location of the Lanta Khola Slide in Sikkim; ***b***, A view of the Lanta Khola Slide from the road level.

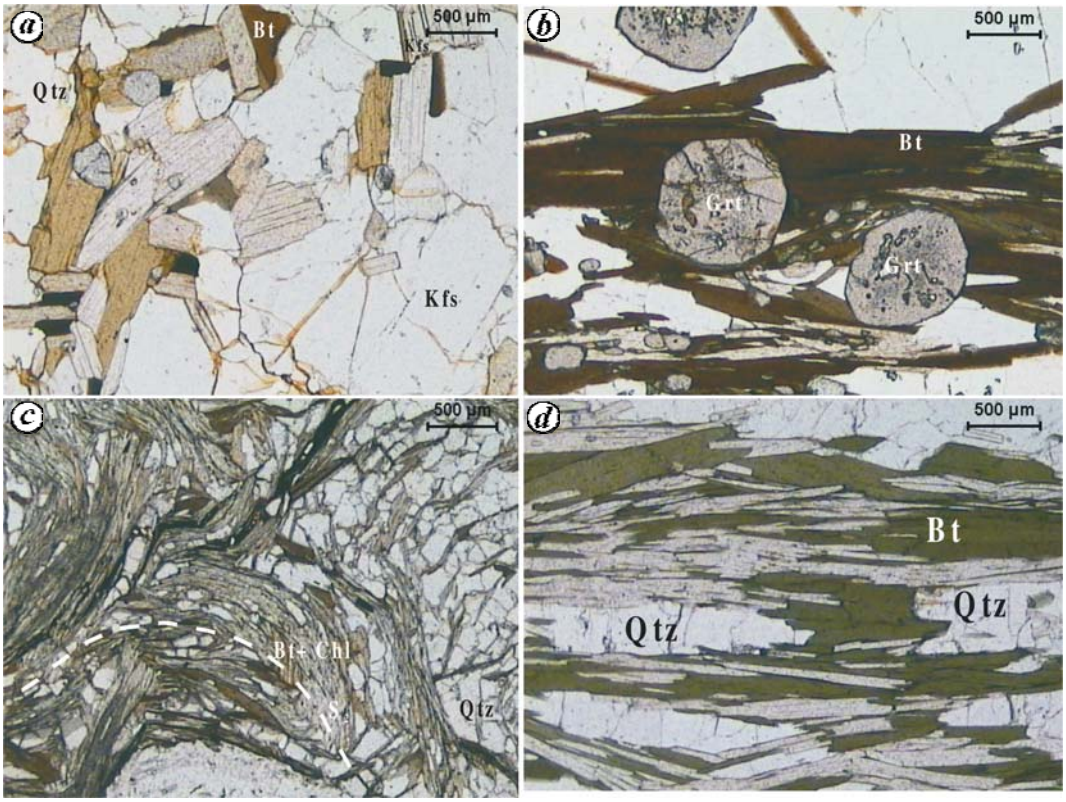

Figure 3. Magnified view of the internal structures of ***a***, Schist at the Lanta Khola Slide. ***b***, Schist away from the slide zone. ***c***, Gneiss at the Lanta Khola Slide. ***d***, Gneiss away from the slide zone.

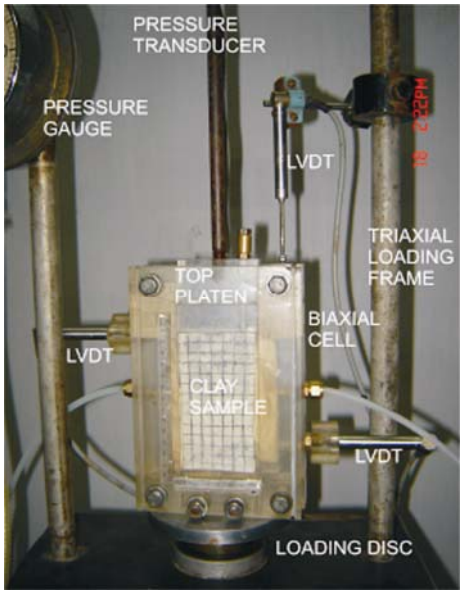

Figure 4. Laboratory biaxial plane strain test set-up.

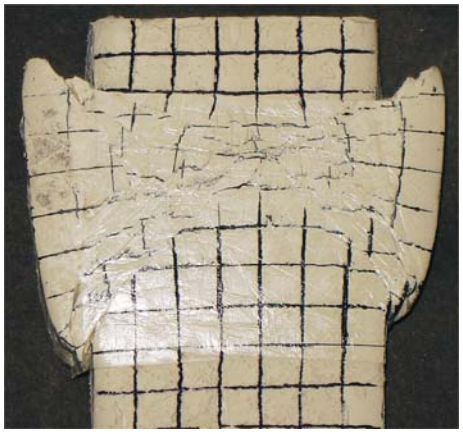

Figure 5. Deformed clay sample at the end of the test (at 16% axial strain).

the vertical direction only between two fixed guides. The uniform pressures on two lateral free sides of the sample are applied pneumatically. Before the tests, square grids of 10×10 mm are imprinted on the soil samples so that deformations and locations of the strain localization within the soil sample can be visualized through the transparent membrane and Perspex plate and measured with the progress of the tests. A stationary digital camera is utilized to record the deformation of the grids with the progress of the axial strain. The average axial stress, deformations in axial and in both horizontal directions are measured by pressure transducer and linear variable differential transformer (LVDTs). The average pore water pressure in the samples is also measured with a pore pressure transducer. The whole plane strain device with soil specimen in it, is mounted on a triaxial loading frame and the soil sample is compressed by lowering the top platen at a constant rate of 1.2 mm per minute (0.86% strain). A

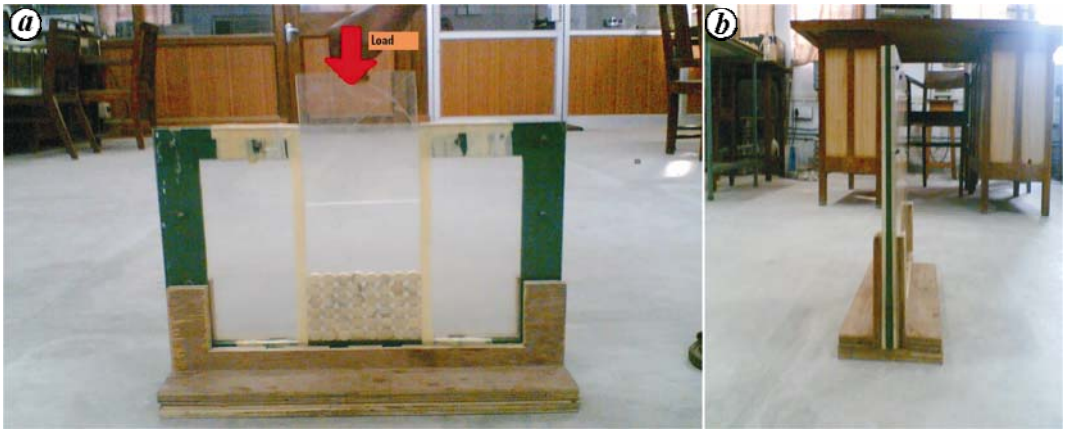

Figure 6. Laboratory model test set-up. ***a***, Front view and ***b***, Side view.

large number of biaxial experiments are performed[23], out of which the result of only one representative test is presented here to keep it simple. The representative test is performed at zero confining pressure and is continued up to 16% axial strain level. Figure 5 shows the deformed sample at the end of the test (that is at 16% axial strain). The localization of strain in 'X' pattern is clearly visible in the soil sample. The strain in different parts of the soil sample is studied from the deformed grids as well as by an indirect technique called anisotropy of magnetic susceptibility (AMS). Both the methods show that the strains within the localized zones are much higher in magnitude than the strains in other areas of the samples[31]. The large strains along the localized zones are also accompanied by rotation of the principal directions. The grains reorient and realign themselves parallel to the strain localization zones. However these kinds of microbehaviours cannot be visualized in the tests. Attempts are made to design a series of laboratory model tests to capture these behaviours during strain localizations.

Laboratory model tests

In the laboratory model tests, the same biaxial plane strain test conditions are simulated. But instead of soil, cylindrical wooden disc, 18.5 mm in diameter and 10 mm in thickness are utilized. The model test set-up (Figure 6) consists of two 396×508 mm Perspex sheets bolted together with 10.5 mm hollow space between them maintained by two C-shaped wooden pieces. The actual test chamber is 396 mm in length and 148 mm in width. The test chamber is filled with the wooden discs. The wooden discs have one of the cylindrical faces painted black and in the other face an arrow mark is painted at the diameter to monitor the rotation during loading. The discs are placed initially in such a way that the arrows are horizontal and facing one single direction. Flexible rubber membranes are tied to the lateral sides of the test chamber to hold the discs in place. However, they do not prevent movement of the discs and allow displacement of the discs when loaded vertically. The bottom of the test chamber is fixed by a 50 mm wooden piece bolted to the frame. The top of the test chamber is free and fitted with a 50 mm Perspex platen which slides down and applies uniform vertical load on the stacked up cylindrical discs. Figure 7 shows the displacement and rotation of the discs at the end of a typical test (at 16% axial strain). Interestingly, the figure shows good resemblance with the theoretical diagram of strain localization given in Figure 1 and the laboratory biaxial test results shown in Figure 5. The 'X' shaped pattern of strain localization is visible even in this macroscale test. The volume of voids (V_v) between the discs, volume of solid (V_s) (that is, volume of the discs) and the void ratios ($e = V_v/V_s$) are calculated. It shows that for the reported test, the average void ratio is 27.3% before the test and they are 18.86%, 32%, 19.9% and 30.4% for the zones A, B, C and D respectively at the end of the test. This implies that the zones A and C are getting compacted while the zones B and D are becoming loose during the compressional vertical loading. This is observed during the biaxial tests also. Figure 6 also shows that almost no rotation and displacement of discs have taken place in Zone C which is also observed in the laboratory biaxial tests. However the rotation of the discs along the 'X' pattern of localized zone is inconclusive. This may be due to the macroscaling of the tests.

Strain localization in the numerical analyses

The objective of the numerical analyses is to simulate the biaxial plane strain tests numerically to see if the formation of shear bands and their patterns as observed in the laboratory tests can also be captured numerically. For this purpose, a coupled plane strain, elasto-plastic finite element package has been developed in-house. The undrained behaviour of kaolinite is simulated by a modified Von Mises yield theory. The modified theory incorporates strain-dependent softening after the yield stress of a material is exceeded. The yield surfaces are represented by a

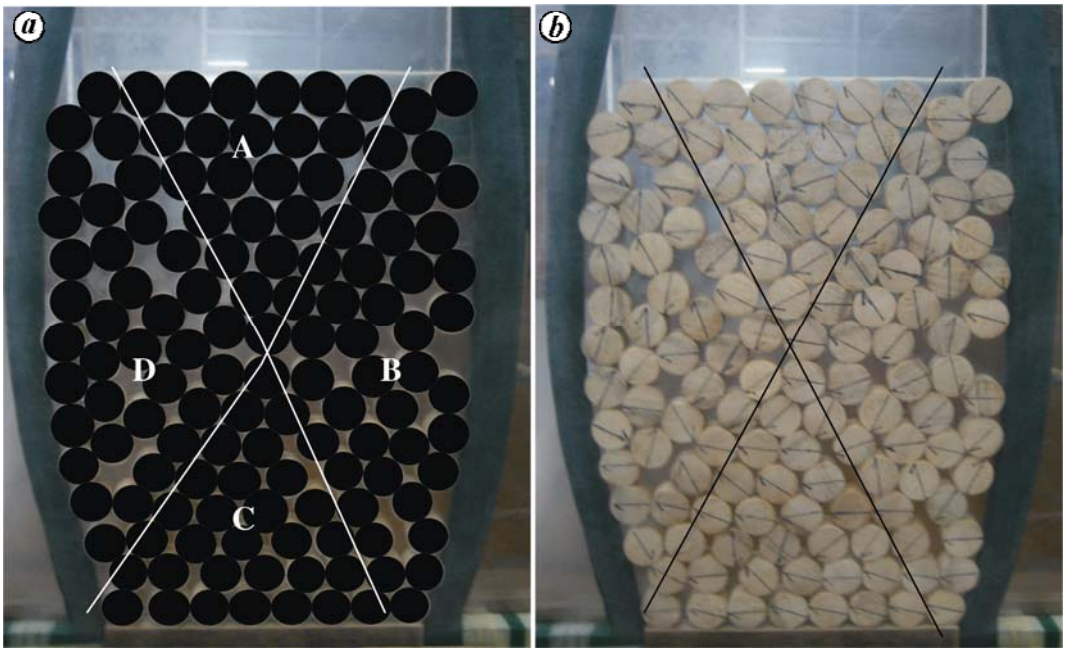

Figure 7. ***a***, Displacement of the discs. ***b***, Rotation of the discs at the end of a model test (at 16% axial strain).

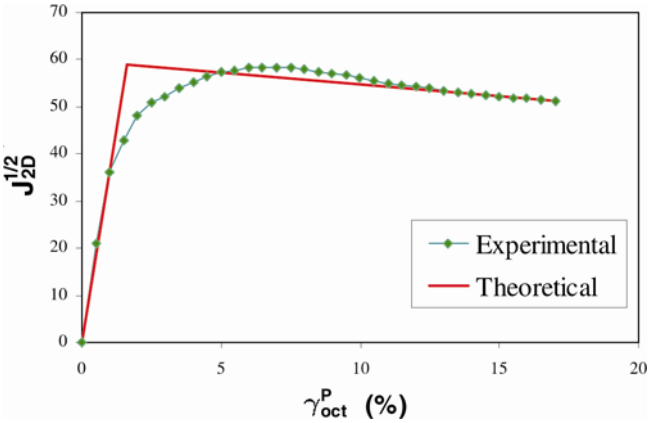

Figure 8. Stress–strain curve obtained from the laboratory biaxial test and that assumed in the finite element analyses.

series of concentric circles. The material yield criterion assumed in the present analyses is expressed as

$$F = F(\sigma, \varepsilon^{P}) = J_{2D}^{1/2} - (\kappa + H\gamma_{oct}^{P}) = 0, \quad (1)$$

where $J_{2D}^{1/2}$ is the 2nd invariant of deviatoric stress, κ the size of initial yield surface, γ_{oct}^{P} the plastic octahedral shear strain and H the plastic hardening modulus.

H, the plastic hardening modulus, represents softening when its value is less than zero and hardening when its value is greater than zero. The main advantage of the present model is that it is simple yet it has the ability to simulate the undrained behaviour of clay very well.

The model requires few standard material parameters like Young's modulus E, shear modulus G, plastic hardening modulus H and Poisson's ratio ν. The stress–strain

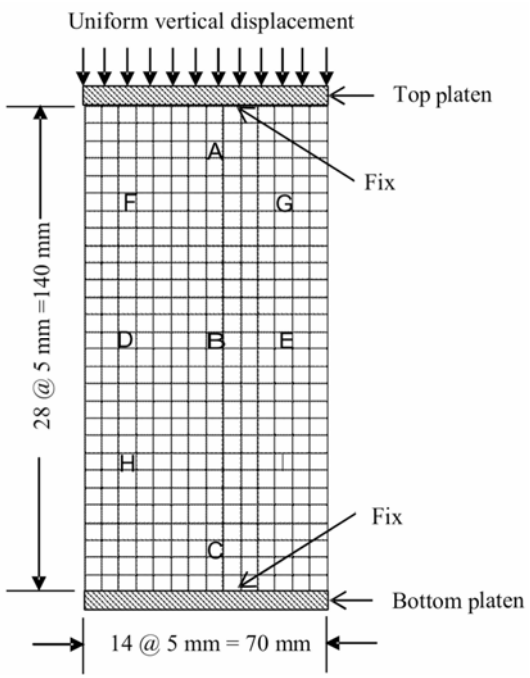

Figure 9. Boundary conditions assumed in the finite element analyses.

behaviour is idealized by a bilinear curve (shown by the solid lines in Figure 8). Figure 8 also shows a comparison between the idealized curve used in the numerical modelling and the curve obtained from the biaxial test. The shear modulus ($2G$) is obtained as the slope of the initial straight line. The slope of the other straight line gives the value of the plastic hardening modulus (H). The stress at the junction of these two straight lines represents the idealized yield stress (κ) of the soil. The Poisson's ratio (ν)

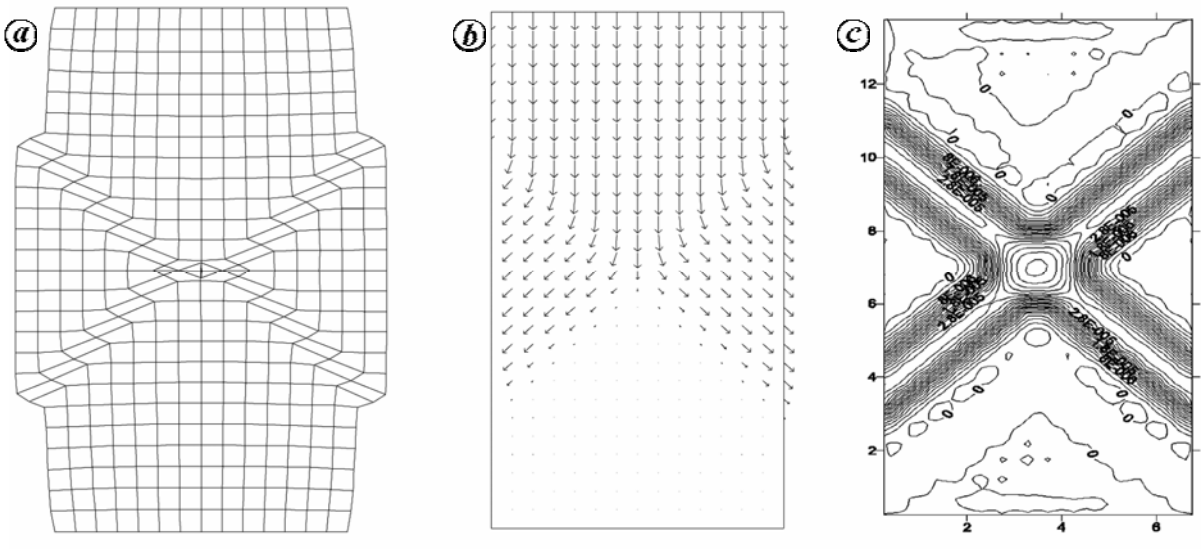

Figure 10. ***a***, Deformed mesh; ***b***, Velocity vectors and ***c***, Strain energy distribution at 16% axial strain in the finite element analysis.

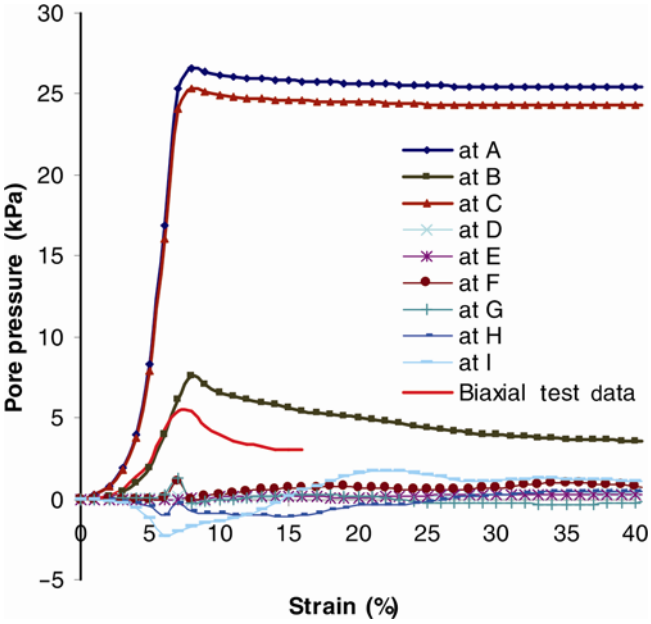

Figure 11. Pore pressure distribution at selected locations within the sample from the finite element analysis and the average pore pressure measured in the soil sample during the biaxial plane strain laboratory test.

is taken as 0.49 for all the undrained tests. The material behaviour is elastic as long as the value of second invariant of deviatoric stress ($J_{2D}^{1/2}$) does not exceed the size of the initial yield surface (κ). From Figure 8, the model parameters for the kaolinite are: Young's modulus (E) = 3122.18 kPa, shear modulus (G) = 1047.71 kPa, yield stress (κ) = 58.79 kPa, non-dimensional softening parameter ($H/2G$) = –0.0360 and Poisson's ratio (ν) = 0.49.

The rectangular soil sample is discretized by five noded constant strain quadrilateral elements whose fifth interior node is removed by static condensation. However, the stresses, strains and convergence are computed at the middle of each element. A total of 435 nodes and 392 elements have been utilized to discretize the 140 × 70 mm soil matrix.

The top and bottom of the soil sample are assumed to be fixed (Figure 9). A uniform vertical axial displacement is applied to the soil sample from the top. The load applied is assumed to be quick so that the soil remains in undrained condition throughout.

The results of the numerical analyses are presented in the form of deformed mesh, velocity vectors and strain energy contours in the soil sample at 16% axial strain (Figure 10). The pore pressures at the selected locations are shown in Figure 11. Figure 9 shows the locations within the soil sample where pore pressures are predicted.

The orientation and the shape of the strain localization bands obtained in the numerical analyses are found to compare reasonably well with the experimental observations. Figure 10 shows the sudden change in directions of strain rate along the bands. It also indicates that all the strain energies (work done) are concentrated along these 'X' shaped bands. This implies that the strains along these bands are several folds higher than those at other locations as suggested in the literature. The pore pressure distribution in the clay matrix during the test shown in Figure 11 is also revealing. It shows that the pore pressures computed near the top and bottom (zones A and C) are much higher than those measured at other places. The pore pressures predicted in zones B and D are negative or very close to zero. This is in agreement with the observations in the model tests. At zones A and C, the void ratios decreased during loading signifying compaction of discs or soil grains in these two zones which will result in increase in pore pressures in saturated undrained condition. Similarly, void ratios in the zones B and D are found to be increasing which signify opening of cracks and loosening of discs or soil grains. This will result in

decrease in pore pressures in these zones under saturated undrained condition. The average pore pressure measured during the biaxial plane strain test is also shown in Figure 11. It is much lower than the pore pressures predicted at the top and bottom of the soil sample and somewhat comparable to the pore pressure predicted at the middle of the sample.

Conclusions

The present study shows that the mechanisms of strain localization reported in the literature have been captured in laboratory tests and in numerical analyses. Similar strain localization and reorientation of microfabrics are surprisingly also observed in highly sheared rocks in landslide-prone areas in Sikkim and also in simple laboratory model tests. It is particularly interesting to note that the strain localizations observed in a landslide, captured in laboratory biaxial plane strain tests and model tests, and predicted by the finite element analyses bear close resemblance to one another. The pore water pressure predicted in a soil sample by the numerical analyses shows that it is significantly different at different places in the same sample. Along the shear bands, the pore water pressures are near zero or negative due to opening of the cracks along these bands. While in the compression zones (at the top and bottom of the sample) in the same sample, they remain positive and relatively high. The pore pressure predicted at the middle of the sample is found to be matching the average pore pressure measured during the laboratory biaxial test on the sample soil.

1. Vardoulakis, I., Stability and bifurcations in geomaterials. *Numerical Methods in Geomechanics*, Balkema, Rotterdam, 1988, pp. 155–168.
2. Arthur, J. R. F., Dunstan, T., Al-Ani, Q. A. J. L. and Assadi, A., Plastic deformation and failure in granular media. *Geotechnique*, 1977, **27**(1), 53–74.
3. Vardoulakis, I., Shear band inclination and shear modulus of sand in biaxial tests. *Int. J. Numer. Anal. Meth. Geomech*., 1980, **4**, 103–119.
4. Vardoulakis, I., Deformation of water-saturated sand: I. Uniform undrained deformation and shear banding. *Geotechnique*, 1996, **46**(3), 441–456.
5. Vardoulakis, I., Deformation of water-saturated sand: II. Effect of pore water flow and shear banding. *Geotechnique*, 1996, **46**(3), 457–472.
6. Mühlhaus, H. B. and Vardoulakis, I., The thickness of shear bands in granular materials. *Geotechnique*, 1987, **37**(3), 271–283.
7. Peters, J. F., Lade, P. V. and Bro, A., Shear band formation in triaxial and plane strain tests. In *Advanced Triaxial Testing of Soil and Rock, ASTM STP 977* (eds Donaghe, R., Chaney, R. and Silver, M.), 1988, pp. 604–627.
8. Drescher, A., Vardoulakis, I. and Han, C., A biaxial apparatus for testing soils. *Geotech. Test. J., GTJODJ*, 1990, **13**(3), 226–234.
9. Finno, R. J., Harris, W. W., Mooney, M. A. and Viggiani, G., Strain localization and undrained steady state of sand. *J. Geotech. Eng., ASCE*, 1996, **122**(6), 462–473.
10. Finno, R. J., Harris, W. W., Mooney, M. A. and Viggiani, G., Shear bands in plane strain compression of loose sand. *Geotechnique*, 1997, **47**, 149–165.
11. Liang, L., Saada, A., Figueroa, L. and Cope, C. T., The use of digital image processing in monitoring shear band development. *Geotech. Test. J., GTJDOJ*, 1997, **20**(3), 324–339.
12. Saada, A. S., Liang, L., Figueroa, J. L. and Cope, C. T., Bifurcation and shear band propagation in sands. *Geotechnique*, 1999, **49**(3), 365–385.
13. Alshibli, Khalid A. and Sture, S., Shear band formation in plane strain experiments of sands. *J. Geotech. Geoenviron. Eng., ASCE*, 2000, **126**(6), 495–503.
14. Alshibli, K. A., Batiste, S. N. and Sture, S., Strain localization in sand: plane strain versus triaxial compression. *J. Geotech. Geoenviron. Eng., ASCE*, 2003, **129**(6), 483–494.
15. Balasubramanium, A. S., Local strains and displacement patterns in triaxial specimens of saturated clay. *Soils Foundations*, 1976, **16**(1), 101–114.
16. Saada, A. S., Bianchini, G. F. and Liang, L., Cracks, bifurcation and shear bands propagation in saturated clays. *Geotechnique*, 1994, **44**(1), 35–64.
17. Topolnicki, M., Gudehus, G. and Mazurkiewicz, B. K., Observed stress–strain behaviour of remoulded saturated clay under plane strain conditions. *Geotechnique*, 1990, **40**(2), 155–187.
18. Finno, R. J. and Rhee, Y., Consolidation, pre- and post-peak shearing responses from internally instrumented biaxial compression device. *Geotech. Test. J., GTJODJ*, 1993, **16**(4), 496–509.
19. Viggiani, G., Finno, R. J. and Harris, W. W., Experimental observations of strain localization in plane strain compression of a stiff clay. In *Localization and Bifurcation Theory for Soils and Rocks* (eds Chambon, R., Desrues, J. and Vardoulakis, I.), Balkema, Rotterdam, 1994.
20. Hicher, P. Y., Wahyudi, H. and Tessier, D., Microstructural analysis of strain localization in clay. *Computers Geotechnics*, 1994, **16**(3), 205–222.
21. Sabatini, P. J. and Finno, R. J., Effect of consolidation on strain localization of soft clays. *Computers Geotechnics*, 1996, **18**(4), 331–339.
22. Lizcano, A., Vardoulakis, I. and Goldscheider, M., Biaxial tests on normally, anisotropically consolidated clay. In *Deformation and Progressive Failure in Geomechanics* (eds Asaoka, A., Adachi, T. and Oka, F.), Pergamon, 1997, pp. 223–228.
23. Sengupta, S. and Sengupta, A., Investigation into shear band formation in clay. *Indian Geotech. J.*, 2004, **34**(2), 141–163.
24. Rudnicki, J. W. and Rice, J. R., Conditions of the localization of deformation in pressure-sensitive dilatant materials. *J. Mech. Phys. Solids*, 1975, **23**, 371–394.
25. Needleman, A., Non-normality and bifurcation in plane strain tension and compression. *J. Mech. Phys. Solids*, 1979, **27**, 231–254.
26. Prevost, J. H., Localization of deformations in elastic–plastic solids. *Int. J. Num. Anal. Meth. Geomech*., 1984, **8**, 187–196.
27. Peric, D., Runesson, K. and Sture, S., Prediction of plastic localization using MRS-Lade model. *J. Geotech. Eng., ASCE*, 1993, **119**(4), 639–661.
28. Wu, W., Non-linear analysis of shear band formation in sand. *Int. J. Num. Anal. Meth. Geomech*., 2000, **24**, 245–263.
29. Lambrecht, M. and Miehe, C., A note on formulas for localized failure of frictional materials in compression and biaxial loading modes. *Int. J. Numer. Anal. Meth. Geomech.*, 2001, **25**, 955–971.
30. Sengupta, A., Anbarasu, K. and Gupta, A., Towards understanding of Lanta Khola landslide in Sikkim Himalayas. 12th International Conference of International Association for Computer Methods and Advances in Geomechanics (IACMAG), Goa, India, 1–6 October 2008, p. 180.
31. Mamtani, M. and Sengupta, A., Anisotropy of magnetic susceptibility analyses of deformed Kaolinite: implications for evaluating landslides. *Int. J. Earth Sci*., 2009, **98**, 1721–1725.

ACKNOWLEDGEMENT. I thank DST, New Delhi for financial support.

Received 27 August 2008; revised accepted 15 March 2010